Measurement of argon (e, $2e$) differential cross sections in the perpendicular plane from 5 to 200 eV above the ionization threshold

Manish Patel and Andrew James Murray*

Photon Science Institute, Department of Physics and Astronomy, University of Manchester, Manchester M13 9PL, United Kingdom

(Received 16 March 2022; accepted 15 April 2022; published 25 April 2022)

New (e, $2e$) differential cross-section measurements from argon are presented in the perpendicular plane, where the incident electron beam is orthogonal to both detected electrons that map out a detection plane as their angles are varied. New data were obtained at energies from 40 to 200 eV above the ionization potential (IP), with the scattered and ejected electrons having equal energies. These data are compared to previous measurements from 5 to 50 eV above the IP as well as to theoretical calculations from different models in this energy range. A significant discrepancy between the prediction of theory and experiment 50 eV above the IP was retested, and the new experiments confirmed the results from previous measurements. Additional data spanning this energy are presented which show a deep minimum in the cross section under these conditions. Results for the evolution of the cross section into the intermediate-energy regime are also discussed.

DOI: 10.1103/PhysRevA.105.042815

I. INTRODUCTION

Ionization of different targets by electron impact is important in areas ranging from understanding the interaction dynamics in plasmas [1,2] to modeling stellar and planetary atmospheres [3,4]. (e, $2e$) coincidence measurements provide the most information about these reaction mechanisms, since they deliver precise cross-section data from an experiment [5]. In (e, $2e$) experiments an incident electron with momentum $\mathbf{k_0}$ collides and interacts with a target; the collision produces scattered and ejected electrons with momenta $\mathbf{k_1}$ and $\mathbf{k_2}$. The experiment detects single electrons and correlates them in time, so as to measure an ionization event. This procedure is repeated many times until a well-defined coincidence signal is produced.

In these ionizing interactions the outgoing electrons can emerge over a wide range of angles and energies, and therefore, a subset of all possible events is measured. The (e, $2e$) process then determines a differential cross section (DCS) that depends on $\mathbf{k_0}$, $\mathbf{k_1}$, and $\mathbf{k_2}$. In the current set of measurements the scattered and ejected electrons were detected orthogonal to the incident electron direction as shown in Fig. 1, so that $\psi = 90^\circ$. The analyzers that select the momenta $\mathbf{k_1}$ and $\mathbf{k_2}$ span the *perpendicular detection plane* and these are moved sequentially to change the mutual angle $\phi = \theta_1 + \theta_2$ as shown. A further constraint in the present studies was that the energies of the detected electrons were set to be equal, so that $E_1 = E_2 = E$. The incident electron energy was thus set to be $E_{\text{inc}} = 2E + \text{IP}$, where IP is the ionization potential of the target. A differential cross section was then determined which depends on both the energy and the mutual angle ϕ.

In perpendicular plane experiments the interaction is sensitive to multiple order scattering processes [6,7] and so the data provides a robust test of different calculations. Models that determine the cross sections for atoms such as H [8] and He [9,10] generally agree well with experiments. For heavier atoms [11,12] and molecules [13] the models do not always predict the cross sections well under different kinematic conditions. This is particularly true for low to intermediate energies. Much of the previous work carried out in Manchester has focused on providing additional data for input to the models in these regimes. An extensive component of these studies included ionization of the stable noble gases, which were investigated in the perpendicular plane and in geometries where the gun angle ψ was varied from 0° to 90° [14–21].

The cross section of He has been investigated theoretically over a wide range of conditions and these models are now considered to be accurate [22]. Neon has been studied in different geometries and the calculations are also found to be in reasonable agreement with experiment [23]. Modeling the collision for Ar, Kr, and Xe is more difficult, since these targets have a large number of bound electrons that can influence the interaction. Calculations have found good agreement with coplanar (e, $2e$) data for these targets at high energies [24]; however, in the low- to intermediate-energy regimes they have met with mixed success, particularly for non-coplanar geometries [11,12].

The motivation for the current work on argon arises from a query by Whelan and co-workers [11] who found a large disagreement between the experimental data in Ref. [14] and their models at an energy of 50 eV above the IP. By contrast, their calculations using a nonrelativistic distorted-wave Born approximation (DWBA) agreed reasonably well at 35 and 40 eV above the IP, as long as postcollisional interactions (PCIs) were not included. These differences prompted the authors to suggest that the experimental results should be remeasured in this regime and that more data were required to establish if the difference was real. PCIs were

*Andrew.Murray@Manchester.ac.uk

 ©2022 American Physical Society

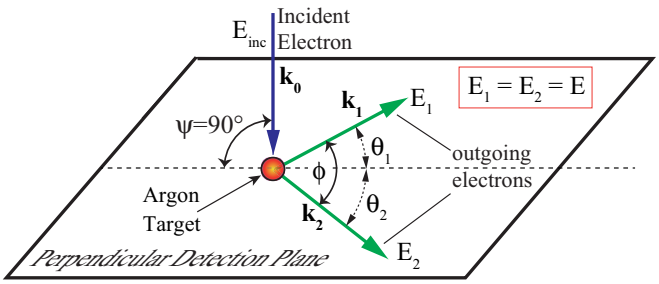

FIG. 1. The perpendicular scattering geometry adopted in the $(e, 2e)$ experiments presented in this paper.

included through the use of both a Gamow factor [25] and the Ward-Macek factor [26]. Both methods provide an approximation to the effect of PCIs and their inclusion for argon was found to overcompensate the effects of electron-electron repulsion. The DWBA model without inclusion of PCIs hence provided the closest agreement to experiment, apart from in the regions near $\phi = 0^\circ$ and 180° where PCIs dominate.

The advantage of DWBA models is that different interaction processes can effectively be switched "on" or "off" by replacing distorted waves with plane waves. This allows different scattering mechanisms to be explored, to try to understand the underlying physical processes involved. By switching the interactions on and off it is possible to investigate different semiclassical ideas for the mechanisms involved. Zhang and co-workers [27] noted that the central peak in the perpendicular plane could be considered as being due to the momentum of the bound electron matching that of the incident electron, so that to preserve momentum both electrons then leave the interaction at a mutual angle of $\phi = 180^\circ$. Peaks observed near $\phi = 90^\circ$ and 270° were considered to arise from elastic scattering of the electron from the atom, followed by a binary collision. Madison and co-workers [6] also used a DWBA model and concluded that the central peak could be explained by triple scattering. In this process the incident electron first scatters elastically into the perpendicular plane, followed by a binary collision with a bound electron. The electron then further scatters elastically from the target to finally emerge at a mutual angle of 180°.

The semiclassical ideas presented in Refs. [6,27] are attractive as they provide a relatively simple explanation of the processes leading to ionization in the perpendicular plane. They do not, however, describe the data well for heavier targets, as seen in Refs. [11,12]. A full quantum calculation is needed to describe the DCS in these cases and the semiclassical ideas appear to break down. Further experimental data are hence desirable to provide a better understanding of the mechanisms that are involved.

Previous perpendicular plane measurements conducted in Manchester from argon were carried out from 5 to 50 eV above the $3\,^2P_{3/2}$ ion state [14]. These data are reproduced here for comparison to the new results which extend the energy to 200 eV above the IP. Data between 40 and 60 eV above the IP have also been obtained with a finer energy mesh than previously adopted, to explore the region of discrepancy between theory and experiment. New results from 60 to 200 eV above the IP were also taken to establish how the DCS varied with angle over a much wider energy range than has been carried out before.

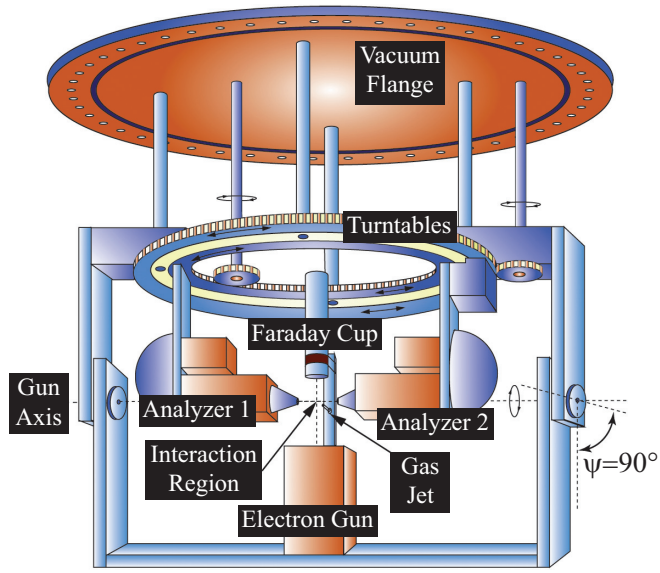

FIG. 2. The $(e, 2e)$ electron spectrometer shown in the perpendicular plane where $\psi = 90^\circ$. The analyzers rotate in the horizontal detection plane via two turntables that are independently controlled. The electron beam passes through the interaction region defined by the electrostatic lenses of the analyzers and gun. The atomic beam is directed into the interaction region through a gas jet as shown.

These experiments took several months to complete due to the very low count rates obtained in the perpendicular plane at higher energies. The spectrometer hence had to be stable for long periods of time. These demands were met using the computer control and optimization techniques that are adopted for the $(e, 2e)$ spectrometer in Manchester, and so for completeness a brief description of the apparatus is given in Sec. II. The results from these studies are then presented in Sec. III, followed by a summary and discussion of other work that is now under way.

II. THE $(e, 2e)$ SPECTROMETER

Figure 2 is a schematic of the spectrometer used for this work. The apparatus is secured from a vacuum flange that connects onto a large nonmagnetic stainless steel chamber. The chamber is lined with a double layer of μ-metal to reduce extraneous magnetic fields to very low levels. All internal components are constructed of nonmagnetic materials that are vacuum compatible. The analyzers span a horizontal detection plane and rotate via computer-controlled turntables. The electron gun rotates on an axis through the center of the plane and is shown in the perpendicular geometry in Fig. 1. The interaction region is defined by electrostatic lenses in the analyzers and the gun. A platinum-iridium gas jet directs atoms into this region and a Faraday cup collects electrons from the gun that pass directly through without collision.

The voltages applied to the lenses in the gun and analyzers are fully computer controlled and computer optimized using LABVIEW [28]. The mutual angle ϕ between the analyzers is adjusted and coincidence timing events are counted by this

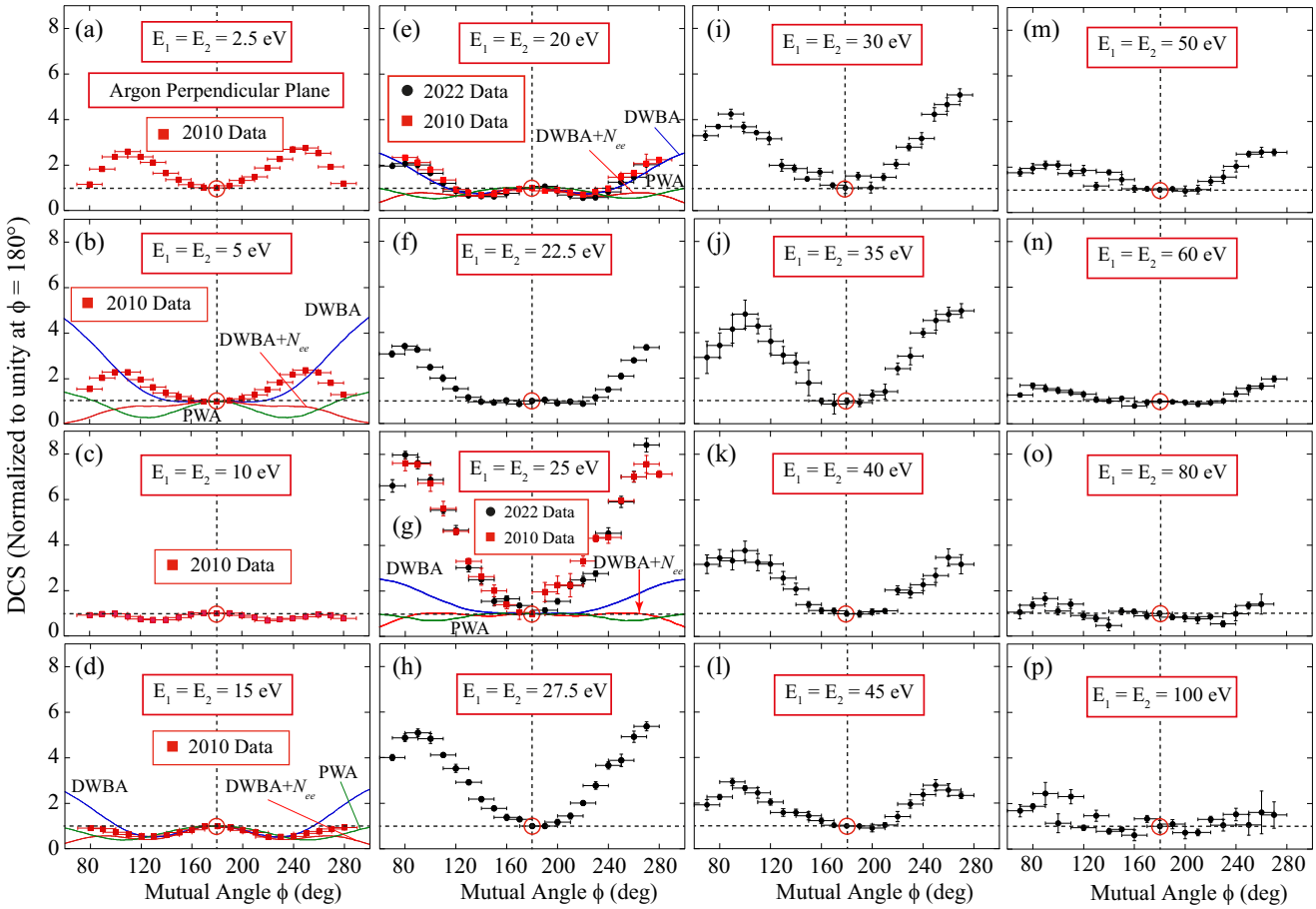

FIG. 3. Evolution of the DCS of argon in the perpendicular plane from (a) 5 eV above the ionization potential to (p) 200 eV above the IP. All measurements are normalized to unity at the mutual angle $\phi = 180^\circ$. The data shown as (red) squares are from measurements taken in 2010 [14], whereas those shown as (black) dots are the new measurements. The calculations of Ref. [11] are also shown as solid curves, as discussed in Sec. III.

program. The vacuum pressure, the Faraday cup current, and the analyzer count rates are logged, with all information stored for analysis as the experiment progresses. The spectrometer can hence operate continuously 24 h each day for many weeks without intervention. This was essential for the experiments detailed here, since the coincidence rates at the higher energies could be as low as a few counts per hour.

The chamber background pressure was 5×10^{-7} mbar. For coincidence measurements argon was directed through the gas jet, so that the pressure increased to 2×10^{-5} mbar. The electron beam current was set to between 70 nA and 3 μA, depending on the incident energy. The incident electron beam had a pencil angle of 2° and the gun was designed to produce a zero beam angle at the interaction region. The analyzer acceptance angles were 3° and they operated so that the overall energy resolution was around 1 eV. It was hence not possible to resolve the $3\,^2P_{1/2}$ and $3\,^2P_{3/2}$ ion states and so the coincidence signals are a contribution from both states. A description of the apparatus and techniques used to optimize the spectrometer can be found in Ref. [29].

The analyzers were each adjusted so that ϕ ranged from $\phi = 70^\circ$ to 270°, this range being limited by the physical size of their input lenses, to avoid collisions. After the analyzer angles were set, the voltages on their lens elements were adjusted automatically to maximize the detected electron count rates, using a modified Nelder-Mead optimization routine. Coincidence data were then accumulated for between 2000 and 12 000 s at each angle, depending on the probability of detection of (*e*, 2*e*) events at that energy and angle. The analyzers were then moved to a new angle and the process was repeated. Once the plane had been mapped in one direction, the analyzers were directed to move in the reverse direction, to again sweep around the plane. Up to 10 full sweeps were made for any given energy. All measurements at each angle were then normalized to a fixed collection time and averaged. The averaged data were then renormalized to unity at $\phi = 180^\circ$.

III. DCS FROM 5 TO 200 eV ABOVE THE IP

The measured cross sections for ionization of argon are presented in Fig. 3 for incident electron energies from 5 to 200 eV above the $3\,^2P_{(1/2,3/2)}$ ion states [14,16]. At each energy the gun angle was set to $\psi = 90^\circ$ and the mutual angle ϕ was adjusted in steps of 10°. The data are normalized to unity at the angle $\phi = 180^\circ$ where the analyzers are opposite each other. The data are hence relative measurements for each energy. Absolute measurements were not attempted due to the difficulty of carrying out this type of measurement under these

kinematic conditions. This is consistent with the previous data that have already been published for this target.

The results from Ref. [14] have been reproduced in Fig. 3 so that a direct comparison can be made between the new measurements and the previous data. This figure also shows how the relative cross section evolves from a low-incident energy of 5 eV above the IP to a high-energy of 200 eV above the IP. The results from the calculations in Ref. [11] are also reproduced to allow comparison between theory and experiment. These include the DWBA calculation with no inclusion of PCI (DWBA), the calculation *with* inclusion of PCI (DWBA + N_{ee}) and when plane waves were used instead of distorted waves (PWA). Results from these models are included for incident energies above the IP of 10 eV [Fig. 3(b)], 30 eV [Fig. 3(d)], 40 eV [Fig. 3(e)], and 50 eV [Fig. 3(g)]. As noted in Ref. [11], the DWBA without PCI gives the closest agreement with the data from $\phi = 120^\circ$ to $\phi = 240^\circ$; however, since PCI is not included, this calculation diverges from the data as the analyzers approach each other. Inclusion of the N_{ee} factor to emulate PCI is clearly too strong an effect, since this calculation further diverges from the data, especially at low and high angles. Its inclusion does, however, ensure that the cross section is zero at $\phi = 0^\circ$ and $\phi = 360^\circ$, which is required for the kinematics chosen here. The plane-wave approximation in general does not emulate the data at any of the energies shown here.

The most striking difference between theory and experiment can be seen at an energy of 50 eV above the IP. It is this difference that motivated the current measurements, as suggested in Ref. [11]. The new experimental data agree well with the older measurements at both 40 eV [Fig. 3(e)] and 50 eV [Fig. 3(g)] above the IP. These results hence show that the models are missing something within the interaction at this energy, leading to this discrepancy. To help elucidate what this mechanism may be, the cross section in this region was further explored over a finer energy grid. These data are presented in Fig. 4 and are discussed below.

Experimental measurements were also taken at higher energies as shown in Figs. 3(h) to 3(p), so that the evolution of the cross section could be further explored beyond previous studies. These measurements are challenging due to the very low coincidence rates that are produced in this region and so there is a reasonable degree of variation in the data. Beyond 50 eV above the IP the cross section is seen to have only a two-peak structure with the lobes decreasing in magnitude as the energy is increased. This trend continues until at 160 eV above the IP the cross section becomes almost flat, with little angular variation as the mutual angle changes. This has also been observed in xenon [30] as well as in some molecular targets in this geometry [31] and so it appears not to be due directly to the target. It is not at present clear why this flattening occurs. Additional calculations are hence required to explain these results.

Detailed survey around 50 eV above the IP

Figure 4 shows the measured DCS over a finer energy grid than adopted in Fig. 3, so that more data in this region are available for comparison to future models. The data for $E_1 = E_2 = 20$ eV [Fig. 4(a)] show a three-peak structure with

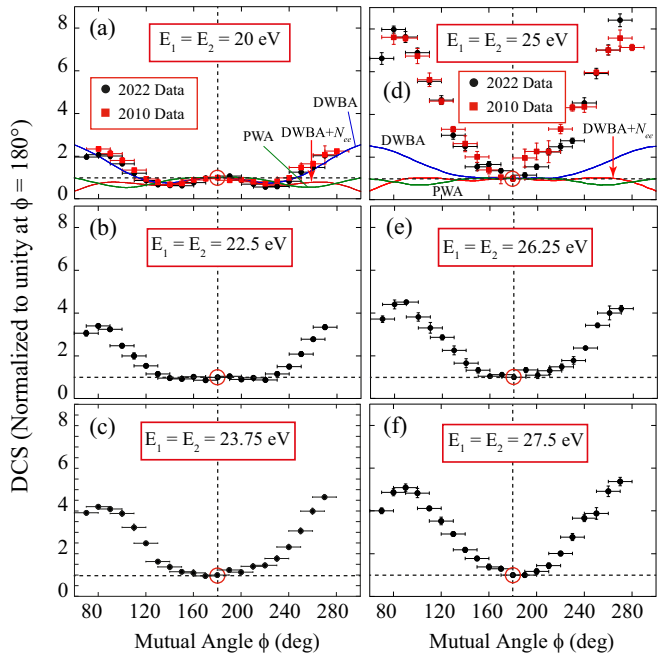

FIG. 4. Detailed survey of the DCS of argon in the perpendicular plane from 40 to 55 eV above the ionization potential. The measurements are again normalized to unity at the mutual angle of 180°. The data shown as (red) squares are from measurements taken in 2010, whereas those shown as (black) dots are the current measurements. The calculations of Whelan and co-workers are shown for 40 and 50 eV above the IP as solid curves, as discussed in Sec. III.

a small central peak at $\phi = 180^\circ$ and two additional peaks at around $\phi = 80^\circ$ and $\phi = 280^\circ$. As noted above, the DCS must be zero at $\phi = 0^\circ$ and $\phi = 360^\circ$ and so these peak amplitudes have to decrease to zero beyond the measured data at these extremities. The DWBA model emulates the data well between $\phi = 80^\circ$ and $\phi = 280^\circ$ at this energy, but does not show the peak structure due to the lack of PCI in this model. Both the previous work from Nixon *et al.* [14] and the new data are in agreement over all angles where measurements were carried out.

The new results 45 eV above the IP are shown in Fig. 4(b). The middle peak is seen to have reduced in amplitude compared to the side lobes, with the data between 140° and 220° being relatively flat. As the energy increases to 47.5 eV above the IP [Fig. 4(c)] the central peak and the flat area have largely disappeared and the DCS in this region decreases compared to that for the side lobes. A small increase in energy to 50 eV [Fig. 4(d)] then shows a rapid decrease in the DCS at $\phi = 180^\circ$ compared to the maxima around $\phi = 90^\circ$ and 270°. The new data and older measurements at this energy are again in agreement. The DWBA, DWBA + N_{ee}, and PWA models do not predict the data at this energy, as has been discussed above. A further increase in energy to 52.5 eV [Fig. 4(e)] and 55 eV [Fig. 4(f)] above the IP shows that the relative magnitude of the side lobes compared to the DCS at $\phi = 180^\circ$ decreases once more. No central structure is observed at energies greater than 45 eV above the IP.

The large changes around $E_1 = E_2 = 25$ eV indicate that an additional process is occurring at this energy that is not

included in the models. The deep minimum relative to the side lobes that is seen here may hence be due to a mechanism first reported experimentally in helium at 64.6 eV for a gun angle of 67.5° [19,32,33]. These helium experiments found that the DCS decreased sharply to zero at this incident beam angle for scattered and ejected electron angles $\theta_1 = \theta_2 = 70°$ (see Fig. 1). It was suggested in Ref. [19] that this deep minimum is due to quantum interference, leading to a zero in the cross section under these non-coplanar kinematic conditions. A second minimum was predicted several years later by Whelan and co-workers [34] from ionization of the inner $2s$ electron in neon. This was subsequently observed experimentally in Manchester [35].

The deep minima that are found in non-coplanar ionization cross sections have been considered theoretically by a number of authors since their discovery, as is discussed in Ref. [11]. This has led to new studies of *quantum vortices* in the wave functions that describe the ionization cross sections. Macek, Briggs, and co-authors [36] first explained the experimental data in Ref. [19] using this approach in 2010. Subsequent theoretical studies have been carried out since that time by a number of authors for both electron and positron impact ionization [37–39], demonstrating the topicality of this new research field. These theories show that the amplitudes of the wave functions that describe the DCS are zero at the center of the vortex, which subsequently leads to the deep minima that are observed in the measured ionization cross sections. The minimum found in the new experimental data presented here may hence arise due to a similar quantum vortex occurring in the ionization of argon. It will be interesting to see if these new models can explain and reproduce the data for this target, under the kinematic conditions adopted here.

IV. SUMMARY AND CONCLUSIONS

In this paper the ionization cross sections for Ar have been presented over a wide range of energies from 5 to 200 eV above the ionization potential of the unresolved $3\,^2P_{(1/2,3/2)}$ ion states. The measurements were carried out in the perpendicular plane, where the incident electron beam is orthogonal to the plane spanned by the outgoing electrons. The detected electrons were selected to have equal energies and the results are presented as a function of the mutual angle ϕ between them. The data are presented on a relative scale with the DCS at $\phi = 180°$ set to unity at each energy. A query by Whelan and co-workers [11] about the reliability of previous data taken in 2010 [14] has now been resolved in favor of the experimental results. Further measurements over a finer energy grid have found that the DCS in this region produces a deep minimum in the cross section that may be related to the presence of a nearby quantum vortex. Further theoretical analysis of the collision is hence required to establish if this is the mechanism that is involved.

New data have also been presented that extend the measurements into the intermediate-energy regime where models such as the distorted-wave Born approximation have proven to be reliable under these kinematic conditions. By providing a comprehensive survey of this region, it is hoped that the calculations can be refined to reveal an accurate description of the interactions that are occurring. The DCS at the higher energies evolves into a broad flat structure with the side lobes seen around $\phi = 90°$ and 270° reducing in magnitude as the energy increases. The broad featureless cross section found at these higher energies has been observed from other targets including Xe and CH_4. The DCS in this region may hence be dominated by the kinematic conditions, rather than by the target structure. More theoretical input is needed to resolve why the DCS evolves in energy as is observed here.

Further measurements are under way to explore these energy regions further, with experiments using Kr now being conducted to extend the existing perpendicular plane data into the higher-energy regime. Results from these experiments will be published in a forthcoming paper.

It will be interesting to see if the new quantum vortex models can predict where vortices occur in other targets. The spectrometer in Manchester has the flexibility to measure the DCS over a wide range of coplanar and non-coplanar kinematics for many different atomic and molecular species in the gas phase, or as are produced from an atomic beam oven. As such it is well placed to measure the cross sections in regions where vortices are predicted to occur in the future.

The data supporting the findings reported in this paper are openly available from the authors through the contact email given above.

ACKNOWLEDGMENTS

We thank the Engineering and Physical Sciences Research Council (EPSRC) for funding through Grant No. R126554. Manish Patel thanks the University of Manchester for providing a Ph.D. scholarship to carry out this work.

[1] V. H. Chaplin, M. Konopliv, T. Simka, L. K. Johnson, R. B. Lobbia, and R. E. Wirz, in *AIAA Propulsion and Energy 2021 Forum* (AIAA, 2021), p. 3378.

[2] Y. Fu, J. Krek, G. M. Parsey, and J. P. Verboncoeur, Phys. Plasmas **25**, 033505 (2018).

[3] R. P. Dufresne and G. Del Zanna, Astron. Astrophys. **626**, A123 (2019).

[4] R. J. Lillis and X. Fang, J. Geophys. Res.: Planets **120**, 1332 (2015).

[5] E. Weigold and I. McCarthy, *Electron Momentum Spectroscopy* (Springer, Berlin, 2012).

[6] O. Al-Hagan, C. Kaiser, D. Madison, and A. J. Murray, Nat. Phys. **5**, 59 (2009).

[7] X. Ren, A. Senftleben, T. Pflüger, A. Dorn, J. Colgan, M. S. Pindzola, O. Al-Hagan, D. H. Madison, I. Bray, D. V. Fursa, and J. Ullrich, Phys. Rev. A **82**, 032712 (2010).

[8] T. Rescigno, M. Baertschy, W. Isaacs, and C. McCurdy, Science **286**, 2474 (1999).

[9] I. Bray, D. V. Fursa, A. S. Kadyrov, A. T. Stelbovics, A. S. Kheifets, and A. M. Mukhamedzhanov, Phys. Rep. **520**, 135 (2012).
[10] J. Colgan, O. Al-Hagan, D. Madison, A. J. Murray, and M. Pindzola, J. Phys. B: At., Mol. Opt. Phys. **42**, 171001 (2009).
[11] F. K. Miller, H. R. J. Walters, and C. T. Whelan, Phys. Rev. A **91**, 012706 (2015).
[12] A. A. Illarionov and A. Stauffer, J. Phys. B: At., Mol. Opt. Phys. **45**, 225202 (2012).
[13] A. I. Lozano, F. Costa, X. Ren, A. Dorn, L. Álvarez, F. Blanco, P. Limão-Vieira, and G. García, Int. J. Mol. Sci. **22**, 4601 (2021).
[14] K. L. Nixon, A. J. Murray, and C. Kaiser, J. Phys. B: At., Mol. Opt. Phys. **43**, 085202 (2010).
[15] K. L. Nixon and A. J. Murray, Phys. Rev. A **85**, 022716 (2012).
[16] K. L. Nixon and A. J. Murray, Phys. Rev. A **87**, 022712 (2013).
[17] A. Murray, M. Woolf, and F. Read, J. Phys. B: At., Mol. Opt. Phys. **25**, 3021 (1992).
[18] A. Murray, N. Bowring, and F. Read, J. Phys. B: At., Mol. Opt. Phys. **33**, 2859 (2000).
[19] A. J. Murray and F. H. Read, Phys. Rev. A **47**, 3724 (1993).
[20] A. J. Murray and F. H. Read, Phys. Rev. Lett. **69**, 2912 (1992).
[21] A. Murray and F. Read, J. Phys. B: At., Mol. Opt. Phys. **33**, L297 (2000).
[22] X. Ren, I. Bray, D. V. Fursa, J. Colgan, M. S. Pindzola, T. Pflüger, A. Senftleben, S. Xu, A. Dorn, and J. Ullrich, Phys. Rev. A **83**, 052711 (2011).
[23] T. Pflüger, O. Zatsarinny, K. Bartschat, A. Senftleben, X. Ren, J. Ullrich, and A. Dorn, Phys. Rev. Lett. **110**, 153202 (2013).
[24] C. T. Whelan, H. Walters, A. Lahmam-Bennani, and H. Ehrhardt (eds.), *(e, 2e) & Related processes*, Nato Science Series C, Vol. 414 (Springer, Berlin, 2012).
[25] G. Gamow, Z. Phys. **51**, 204 (1928).
[26] S. J. Ward and J. H. Macek, Phys. Rev. A **49**, 1049 (1994).
[27] X. Zhang, C. T. Whelan, and W. H. R. J, J. Phys. B: At., Mol. Opt. Phys. **23**, L173 (1990).
[28] M. Patel, A. Sakaamini, M. Harvey, and A. J. Murray, Rev. Sci. Instrum. **91**, 103104 (2020).
[29] A. J. Murray, B. C. H. Turton, and F. H. Read, Rev. Sci. Instrum. **63**, 3346 (1992).
[30] M. Patel, M. Harvey, A. Sakaamini, and A. J. Murray, Phys. Rev. A, **105**, 032818 (2022).
[31] M. Harvey, A. Sakaamini, M. Patel, S. Amami, D. Madison, and A. Murray, J. Chem. Phys. **151**, 194305 (2019).
[32] A. Murray and F. Read, J. Phys. B: At., Mol. Opt. Phys. **26**, L359 (1993).
[33] N. Bowring, F. Read, and A. Murray, J. Phys. B: At., Mol. Opt. Phys. **32**, L57 (1999).
[34] J. Rasch, C. T. Whelan, R. J. Allan, S. P. Lucey, and H. R. J. Walters, Phys. Rev. A **56**, 1379 (1997).
[35] A. J. Murray and F. H. Read, Phys. Rev. A **63**, 012714 (2000).
[36] J. H. Macek, J. B. Sternberg, S. Y. Ovchinnikov, and J. S. Briggs, Phys. Rev. Lett. **104**, 033201 (2010).
[37] F. Navarrete and R. Barrachina, Nucl. Instrum. Methods Phys. Res., Sect. B **369**, 72 (2016).
[38] A. Alrowaily, S. Ward, and P. van Reeth, J. Phys. B: At., Mol. Opt. Phys. **52**, 205201 (2019).
[39] C. DeMars, S. Ward, J. Colgan, S. Amami, and D. Madison, Atoms **8**, 26 (2020).